Project no. 606953

MarcoPolo

Monitoring and Assessment of Regional air quality in China using space Observations.

Project Of Long-term sino-european co-Operation

Type of funding scheme: Collaborative Project - Small or medium-scale focused research project
Work programme topics addressed: SPA.2013.3.2-01: Cooperation with third countries

Deliverable D3.4 (PU)

< SO_2 Emissions Estimates over China>

Version: 1.0

Due date of final deliverable: project month 24
Actual submission date: project month 34

Organisation name of lead contractor for this deliverable: Aristotle University of Thessaloniki

Document Status sheet	
Lead Authors	MariLiza Koukouli
Contributing Authors	Dimitris Balis
Reviewed by	Ronald van der A
Distribution list	Project partners and EC

Document Change Record			
Date	***Issue***	***Pages affected***	***Description***
Friday 07 October 2016	1.0	all	<First version of the report initialised>

Table of Contents

1 Introduction

With the rapid development of the Chinese economy since 2000, sulfur dioxide, SO_2, emissions from China have been of increasing global concern. There have been indications that the emission growth rate slowed around 2005 and that emissions began to decrease after 2006, mainly due to the wide application of flue-gas desulfurization devices in power plants. However due to the differences in growth rate among the many Chinese Provinces, it remains to be seen whether this decreasing trend can be verified for the entire domain. In this study we use space-based observations of SO_2 columns from the Ozone Monitoring Instrument on board the Aura satellite, OMI/Aura, to derive monthly top-down SO_2 emissions over China via inverse modeling with the CHIMERE chemical transport model. The driving SO_2 emissions have been provided by the Multi-resolution Emission Inventory for China (MEIC) model. In MEIC, the SO_2 sources are further partitioned among industry, power and residential provenances. This study aims at providing updated SO_2 emissions, based on satellite observations, which may later be used to update existing chemical transport model results.

During the past decade or so, with the rapid improvement of satellite instrumentation as well as novel algorithmic development, the monitoring of atmospheric pollutant emissions on a global scale has shifted turned towards the satellite community. Especially China, with its rapid economic growth, became a focal point of many studies, especially for the NOx family of gases [e.g. Zhang et al., 2007; Gu et al., 2014]. In this framework the estimation of sulphur dioxide, SO_2, emissions over China, as provided by satellite observations is attempted. The methodology followed, discussed in Section 3, requires an existing, *apriori*, emission inventory [presented in Section 2.1], chemistry-transport modelling of said emissions in order to extract an SO_2 modelled field [Section 2.2] and the satellite SO_2 observations [Section 2.3.] The calculated top-down emission field is presented and discussed in Section 3.1 whereas the final, *aposteriori*, updated emission inventory is shown in Section 3.2.

2 Data and Methodology

2.1 The MEIC emission inventory

The Multi-resolution Emission Inventory for China, MEIC, compiled by Tsinghua University, Beijing, China, is a production-based inventory, updated from the widely used INTEX-B data set (Zhang et al., 2009). The inventory covers 31 provinces or autonomous regions, 10 pollutants, such as SO_2, NOx, CO, PM 2.5, PM10, ammonia, organic

carbon, etc., and 700 emission source categories. In this study, the 2010 SO_2 emission inventory has been extracted from the http://www.meicmodel.org repository on a monthly basis and a 0.25°x0.25° grid. The SO_2 emissions, in Mg/month, are provided for four sectors: power, industry, residential, and transportation. The domain studied here spans from 102°E to 132°E and from 15°N to 55°N. In **Fig. 1**, the emission separated in the four sectors are given for the month of August 2013, with industry and power [first row] producing the highest yields, followed by residential consumption [bottom left] and transportation [bottom right.]

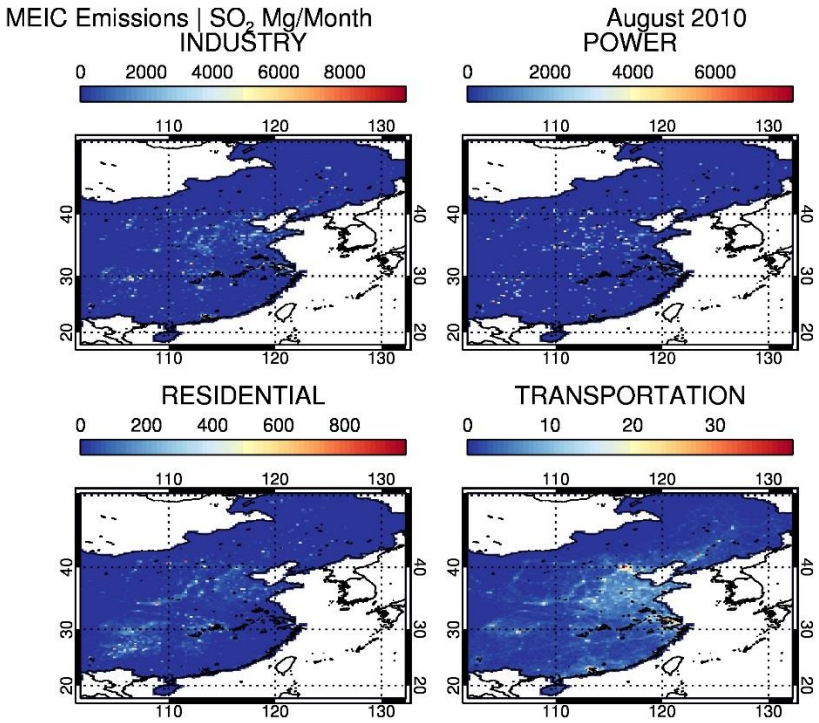

Fig. 1. The MEIC emission inventory for August 2010 in Mg per month for four sectors: upper left, industry; upper right, power; lower left, residential and lower right, transportation. Please note the different colour scales.

2.2 The OMI/Aura SO_2 observations

Daily OMI/Aura planetary boundary layer SO_2 observations for year 2013 and the same domain discussed above have been provided by the Belgian Institute of Aeronomie, BIRA, algorithm [Theys et al., 2015]. OMI is a nadir, UV-Vis-viewing instrument, on board the Aura satellite with a local solar overpass time of 13:30L.T. and a 13 km x 25

km pixel size [Levelt, et al., 2006]. The retrieval of SO_2 vertical column densities, VCDs, using the BIRA algorithm is achieved by applying the Differential Optical Absorption Spectroscopy technique to the measured spectra in the 312–326 nm wavelength range.

The observations were filtered for high solar zenith angles over 70°, high cloud fractions over 20% and, using robust algorithm flagging, were averaged onto a 0.25°x0.25° monthly grid using a 0.75° smoothing average box. In **Fig. 2**, left, an example of the month of August 2013 is shown where the SO_2 load in Dobson Units, D.U., is given.

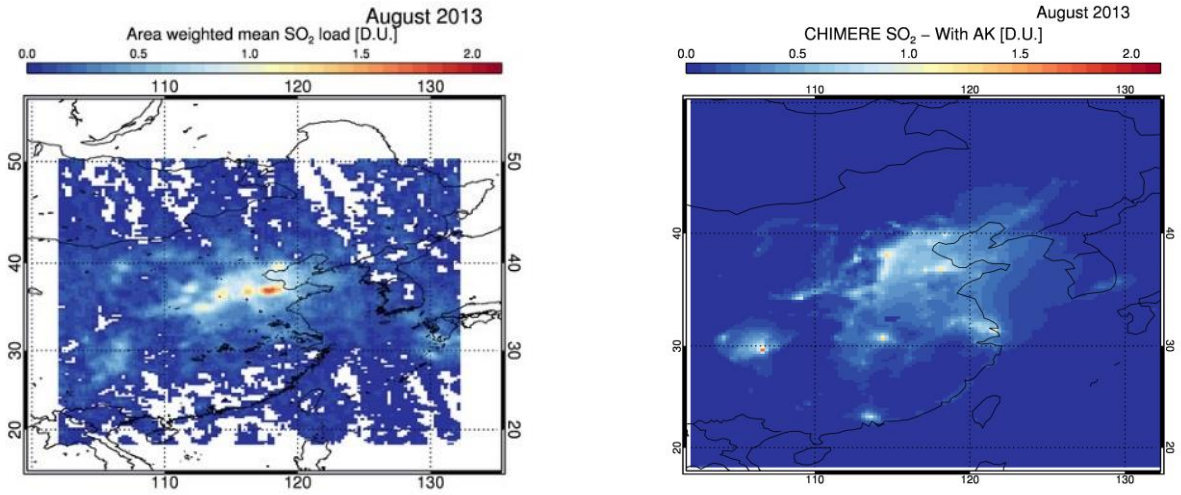

Fig. 2. Left. The OMI/Aura area weighted gridded mean SO_2 observations for August 2013 in D.U. Right: The CHIMERE model SO_2 output for August 2013 in D.U. based on the MEIC emissions shown in Fig. 1.

2.3 The CHIMERE model SO_2 output

CHIMERE is an Eulerian off-line chemistry-transport model, CTM (Menut et al., 2013). External forcings are required to run a simulation: meteorological fields, primary pollutant emissions and chemical boundary conditions. Using these input data, CHIMERE calculates and provides the atmospheric concentrations of tens of gas-phase and aerosol species over local to continental domains (from 1 km to 1 degree resolution). In this work, the CHIMERE model version v2013b was applied to the domain 102°E - 132°E and 15°N - 55°N for year 2013 for a 0.25°x0.25°

resolution. The anthropogenic emission inventory used in this CHIMERE run is the MEIC inventory discussed in Section 2.1, whereas the biogenic emission results from the Model of Emissions of Gases and Aerosols from Nature, MEGANv2.1, dataset (Guenther et al., 2012.) The meteorological input has been extracted from the European Centre for Medium-Range Weather Forecasts, ECMWF, operational data. The output SO_2 profile is given in 8 vertical levels, from surface up to 500hPa, which were integrated using the standard atmospheric equations to produce SO_2 columns in D.U. The month of August 2013 is shown as example in **Fig. 2**, right.

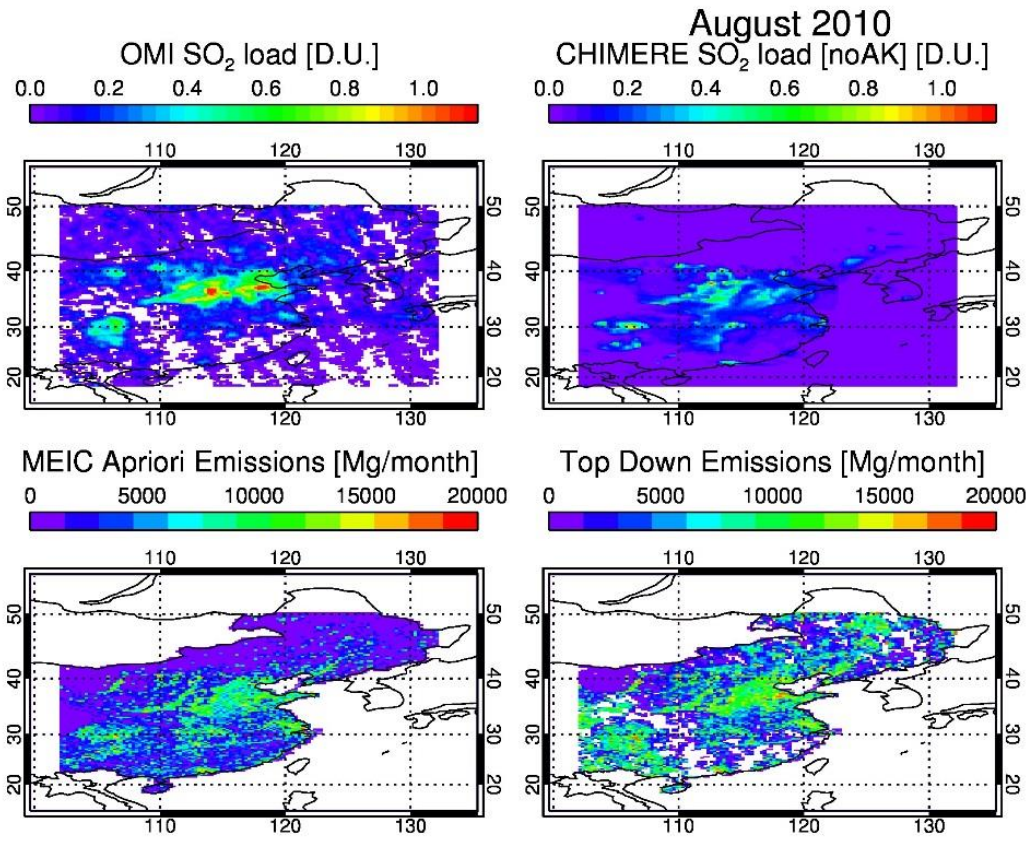

Fig. 3. The top-down emission method applied to the month of August 2013. Upper left, the OMI SO_2 load in D.U.; upper right, the CHIMERE SO_2 model output in D.U.; lower left, the MEIC apriori SO_2 emissions and lower right in Mg/Month, the top-down SO_2 emission inventory in Mg/Month.

3 Results

3.1 Calculating the top-down emission inventory

$$E_t = E_a * \frac{\Omega_t}{\Omega_a} \qquad \textbf{Equation 1}$$

Following the mass balance method (Leue et al., 2001) as described by Martin et al. (2003 and 2006), the top-down SO_2 emission inventory, E_t, may be calculated as a function of the *apriori* emission inventory, E_a, a CTM SO_2 field, Ω_a, based on the same *apriori* emissions and the satellite SO_2 observations, Ω_t, as shown in Eq. 1. In our case, E_a is provided by the MEIC emission inventory [Section 2.1], Ω_a by the CHIMERE model output [Section 2.3] and Ω_t by the OMI/Aura BIRA data [Section 2.2]. The associated top-down SO_2 emission inventory error, ε_t, is calculated according to Eq. 2, where, ε_a, denotes the error in the apriori emission field, E_a, assumed here to be 50% of the original emissions and $\varepsilon_{\Omega t}$ denotes the error in the OMI SO_2 observations calculated as discussed in Theys et al., 2015.

$$\varepsilon_t^2 = \left(\frac{\Omega_t}{\Omega_a} * \varepsilon_a\right)^2 + \left(\frac{E_a}{\Omega_a} * \varepsilon_{\Omega t}\right)^2 \qquad \textbf{Equation 2}$$

The top-down emission inventory is given in the bottom left panel of **Fig. 3** in Mg/month [bottom right] for the month of August 2010. The OMI SO_2 observations are shown in the upper left, where any white areas within the domain studied denote areas of no satellite observations for that month. In the upper right, the CHIMERE SO_2 model output is presented, where areas in purple denote near-zero SO_2 concentration. In the bottom left, the MEIC apriori SO_2 emissions are shown for all four sectors totaled. As expected, the top-down emissions follow closely the patterns of the *apriori* emissions albeit with higher absolute levels and also high emissions in regions where the satellite observations note a strong SO_2 source and the CHIMERE model was not able to capture that load.

3.2 Calculating the aposteriori emission inventory

The calculated *top-down* emission inventory, E_t, may be combined with the *apriori* emission inventory, E_a, to provide an *aposteriori* emission inventory, E_p, following the maximum likelihood theory and a log-normal distribution of errors. In Equation 3 the calculation of the *aposteriori* emission inventory is given, and its associated errors in. Equation 4. Hence, in this methodology, the original bottom-up emission inventory is integrated with the top-down satellite observations, weighted by their respective errors, and using modeling outputs as background field, in order to constraint, update and provide new emissions estimates. It also follows that since the *apriori* emission field is weighted by the top-down emission field error, and vice versa, the *aposteriori* will depend mostly on the *apriori* should the errors of the top-down be too large, and vice versa. In that way, it is assured that at locations where the satellite observations are too sparse or the information content in the SO_2 load too low, the *aposteriori* emission field will revert back to the *apriori.*

$$\ln E_p = \frac{\ln E_a \, (\ln \varepsilon_t)^2 + \ln E_t \, (\ln \varepsilon_\alpha)^2}{(\ln \varepsilon_t)^2 + (\ln \varepsilon_a)^2} \qquad \textbf{Equation 3}$$

$$(\ln \varepsilon_p)^{-2} = (\ln \varepsilon_t)^{-2} + (\ln \varepsilon_a)^{-2} \qquad \textbf{Equation 4}$$

An example of the aposteriori *emissions* calculated with the methodology and input parameters discussed above is shown in Fig. 4. For the month of August 2010, the original, bottom-up, MEIC emission field is shown in the top left, whereas the *aposteriori* emissions in the top right. Theie percentage differences and their absolute differences are shown in the bottom row, left and right, respectively.

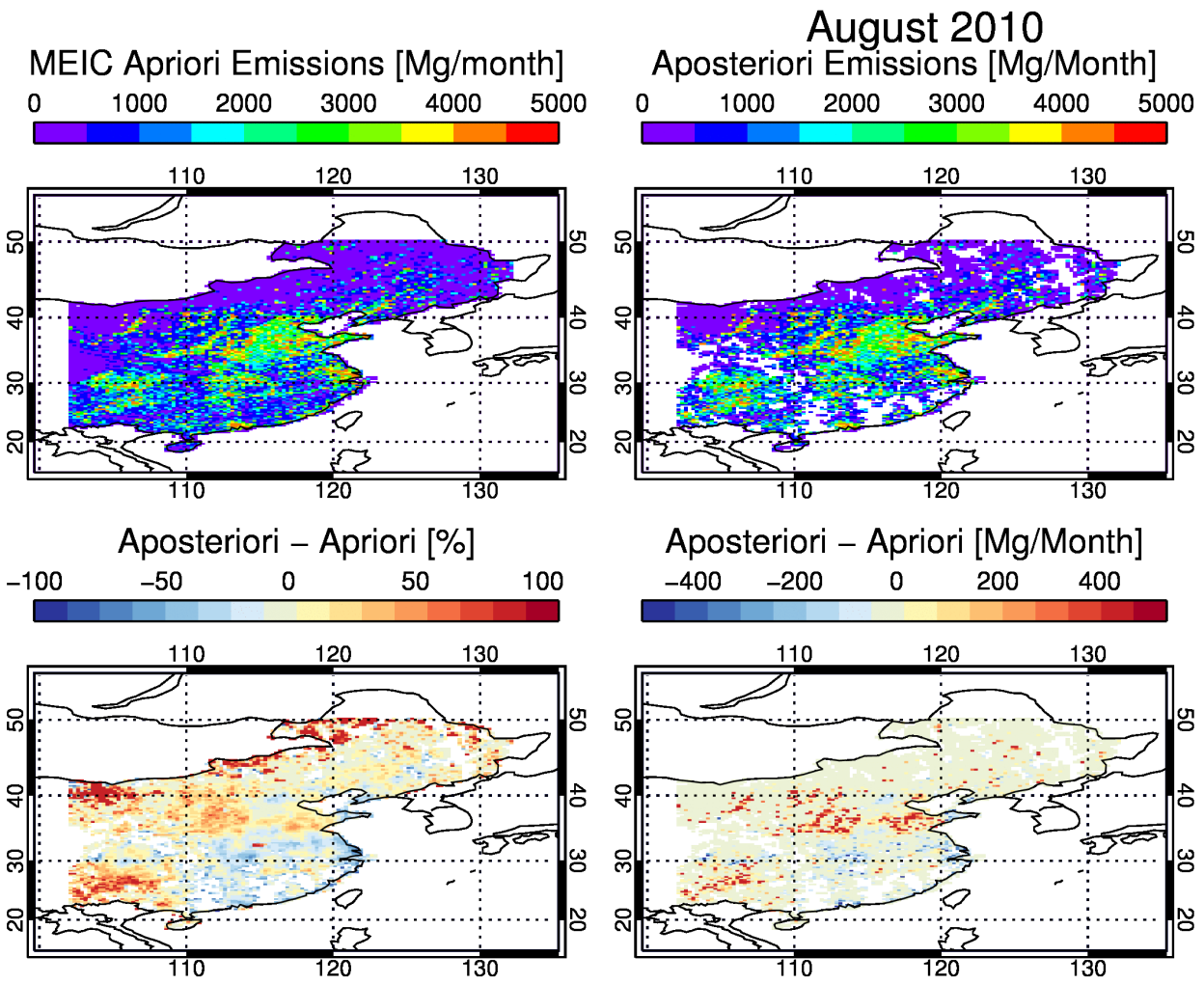

Fig. 4. The original, bottom-up, MEIC emissions [upper left] compared to the aposteriori emissions calculated in this work [upper right] are shown for August 2010 in Mg/month. The percentage differences and the absolute differences are shown in the bottom row, left and right, respectively.

4 Conclusions

In this work, the first step towards creating a satellite-based emission inventory for the SO_2 load over China has been presented using the month of August 2010 as example and input from the CHIMERE CTM, the MEIC emission inventory and the OMI/Aura observations. The technique applied has already been verified in previous works,

mainly for NOx, and is furthered into calculating an *aposteriori* emission inventory which may then be used as input to a CTM run in lieu of the a*priori* emission field.

Description of emission inventory provided to MarcoPolo

The aposteriori SO_2 emissions for year 2014, in the domain from 102°E to 132°E and from 15°N to 55°N, in a 0.25°x0.25° spatial resolution and monthly temporal resolution, have been provided to the MarcoPolo project and can be found at http://www.marcopolo-panda.eu/wp/data/inventory/MarcoPoloInventory_v0.1.zip.

The netcdf data files contain the following structure:

- Dimensions
  - lat = 129
  - lon = 121
- Attributes
  - author = "MariLiza Koukouli"
  - contact information = "mariliza@auth.gr"
  - institution = "Laboratory of Atmospheric Physics, Aristotle University of Thessaloniki"
  - time frame = "2014"
  - sector classification = "total emissions"
  - emis_cat_name = "sulphur dioxide emissions"
  - source_type_name = "sulphur dioxide emissions"
  - pollutant_description = "updated sulphur dioxide emissions based on the CHIMERE model running the MEIC emissions and the OMI/Aura observations"
  - unit_emissions = "Mg/month"
  - nodata_value = "-9999.0"
- Variables
  - float emissions(lon, lat)

In Appendix I and Appendix II the emission inventory is presented for the full twelve months of 2014.

Appendices.

Appendix I. The monthly emission fields as calculated in this work over China for year 2014. From left to right and top to bottom, the twelve months of the year are shown. In each panel: top left, the OMI/Aura SO_2 load in D.U.; top right, the CHIMERE SO_2 load in D.U.; bottom left, the *aposteriori* emissions in Mg/month and in the bottom right, the difference to the *apriori* MEIC emissions in %.

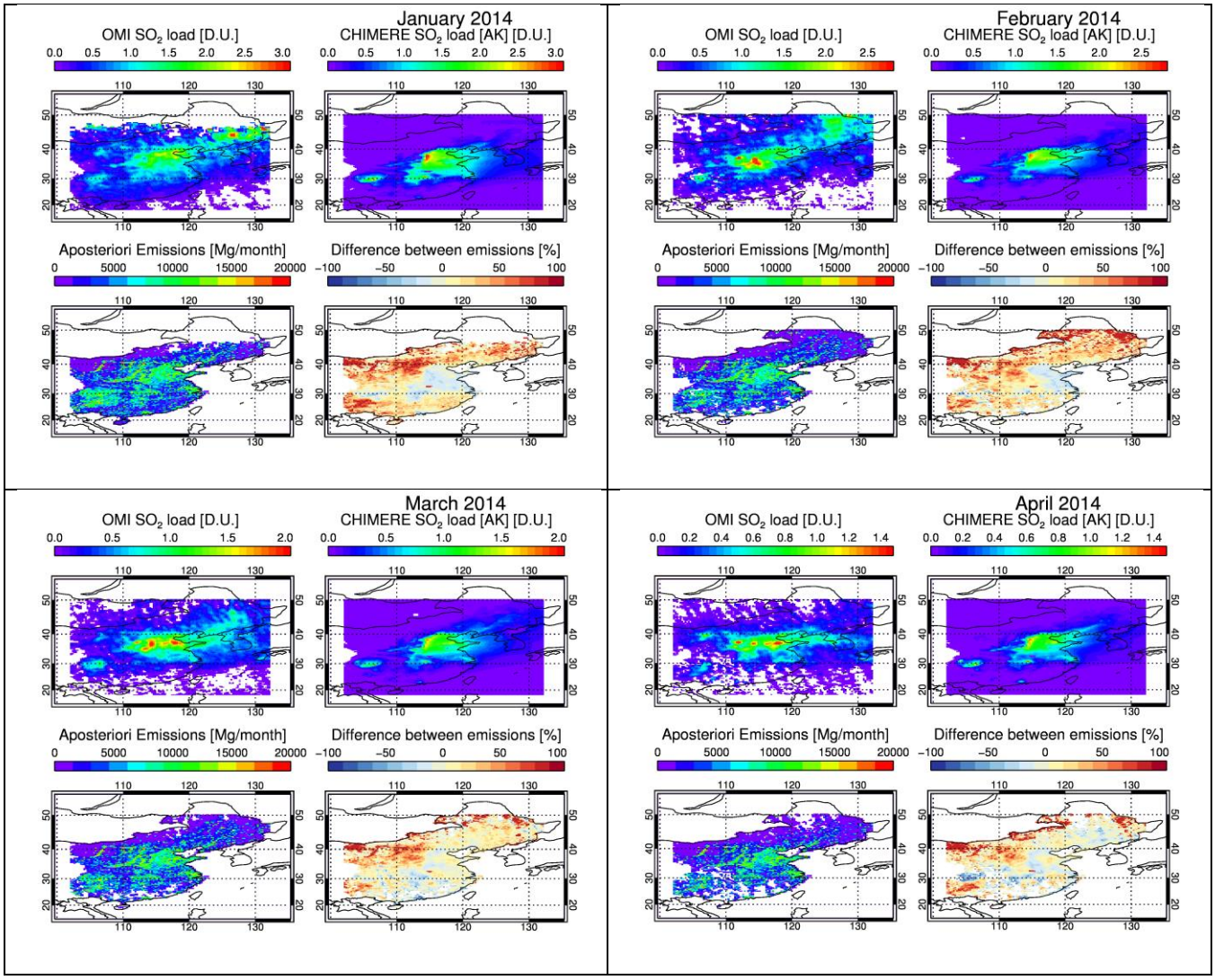

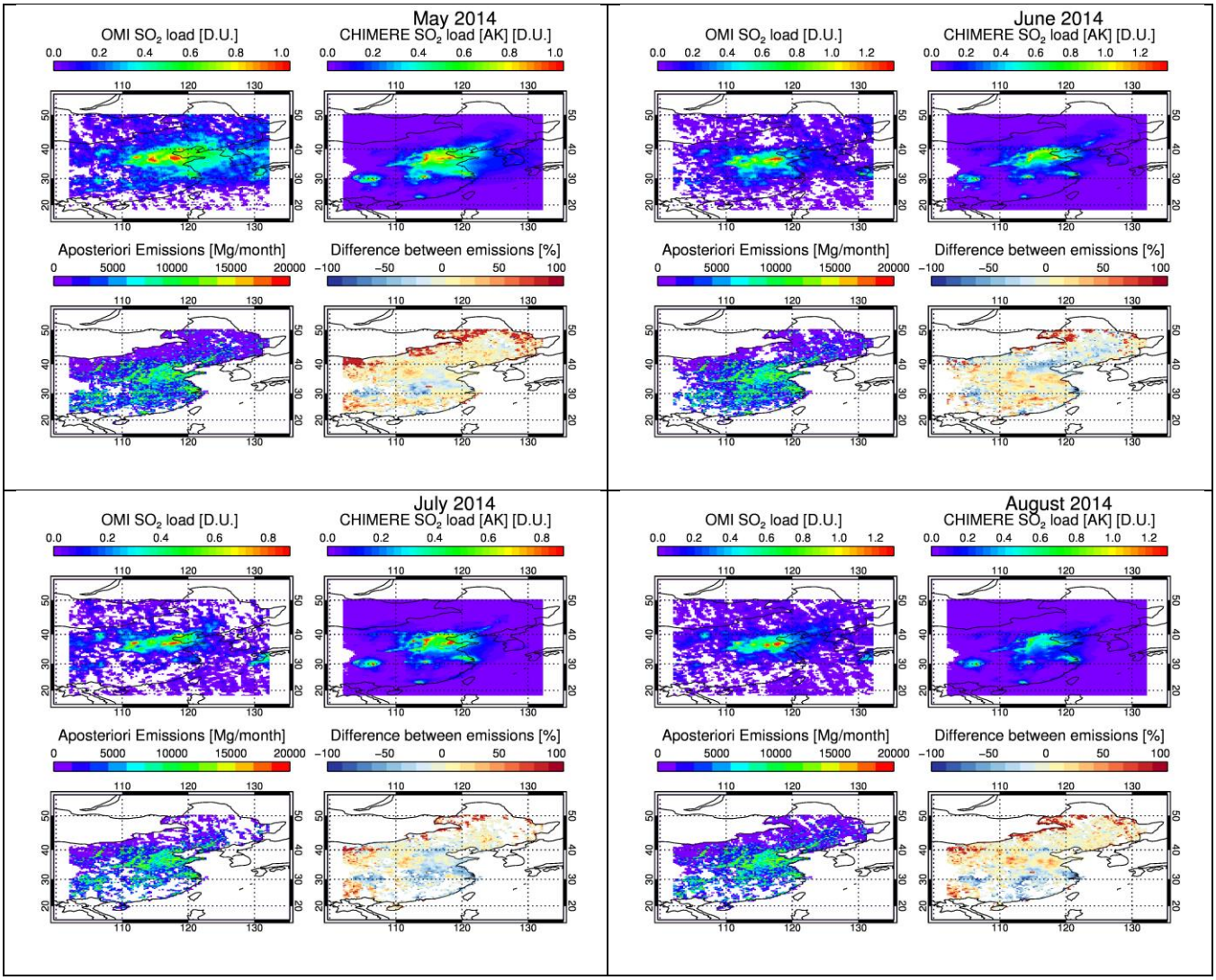
May 2014
OMI SO2 load [D.U.]
CHIMERE SO2 load [AK] [D.U.]
Aposteriori Emissions [Mg/month]
Difference between emissions [%]
June 2014
OMI SO2 load [D.U.]
CHIMERE SO2 load [AK] [D.U.]
Aposteriori Emissions [Mg/month]
Difference between emissions [%]
July 2014
OMI SO2 load [D.U.]
CHIMERE SO2 load [AK] [D.U.]
Aposteriori Emissions [Mg/month]
Difference between emissions [%]
August 2014
OMI SO2 load [D.U.]
CHIMERE SO2 load [AK] [D.U.]
Aposteriori Emissions [Mg/month]
Difference between emissions [%]

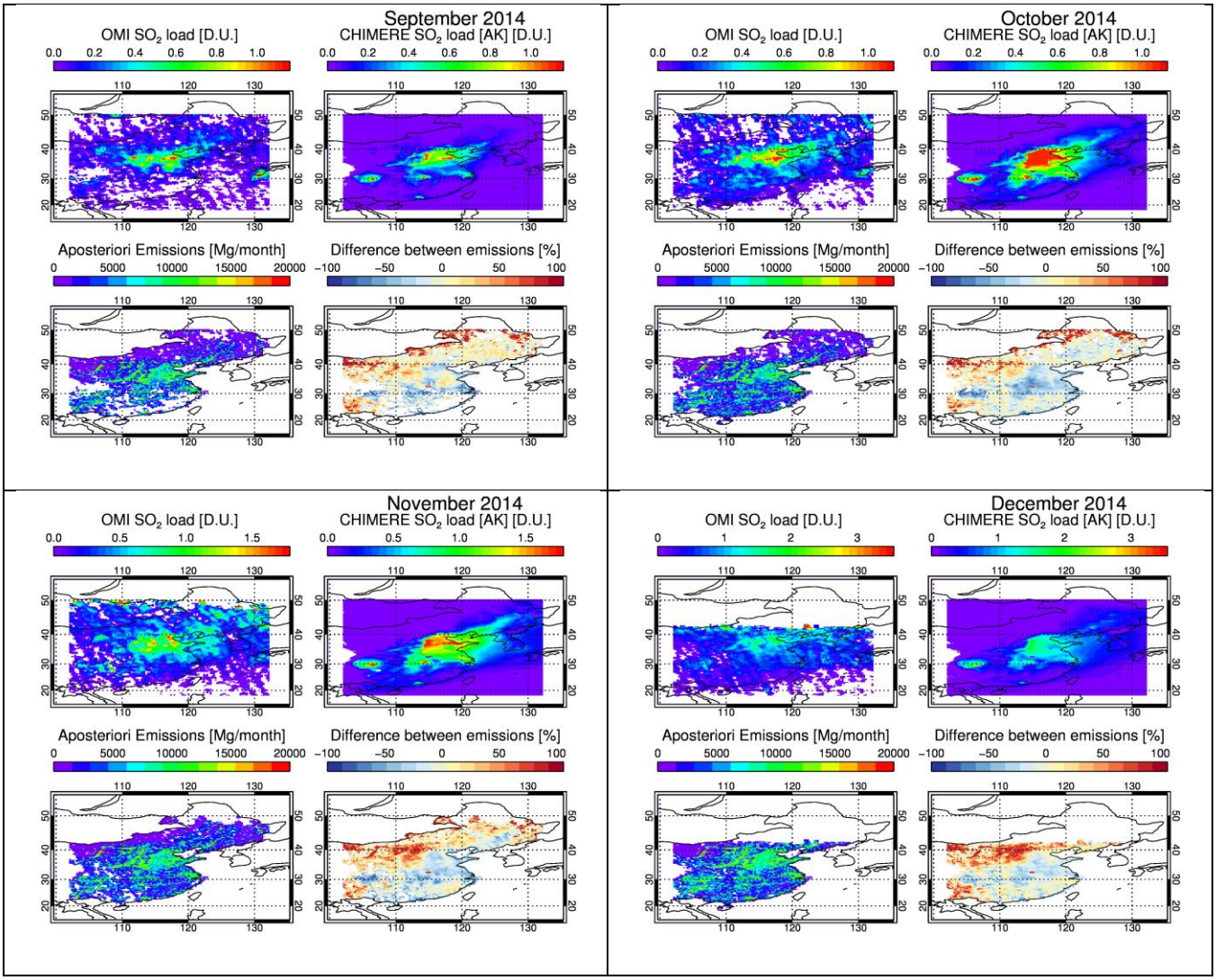
September 2014
OMI SO2 load [D.U.]
CHIMERE SO2 load [AK] [D.U.]
Aposteriori Emissions [Mg/month]
Difference between emissions [%]
October 2014
OMI SO2 load [D.U.]
CHIMERE SO2 load [AK] [D.U.]
Aposteriori Emissions [Mg/month]
Difference between emissions [%]
November 2014
OMI SO2 load [D.U.]
CHIMERE SO2 load [AK] [D.U.]
Aposteriori Emissions [Mg/month]
Difference between emissions [%]
December 2014
OMI SO2 load [D.U.]
CHIMERE SO2 load [AK] [D.U.]
Aposteriori Emissions [Mg/month]
Difference between emissions [%]

Appendix II. The monthly emission fields as calculated in this work over China for year 2014. From left to right and top to bottom, the twelve months of the year are shown. In each panel: top left, the MEIC *apriori* emissions in Mg/month; top right, the aposteriori emissions in Mg/month; bottom left, the difference between emission inventories in Mg/month and in the bottom right, the difference in %.

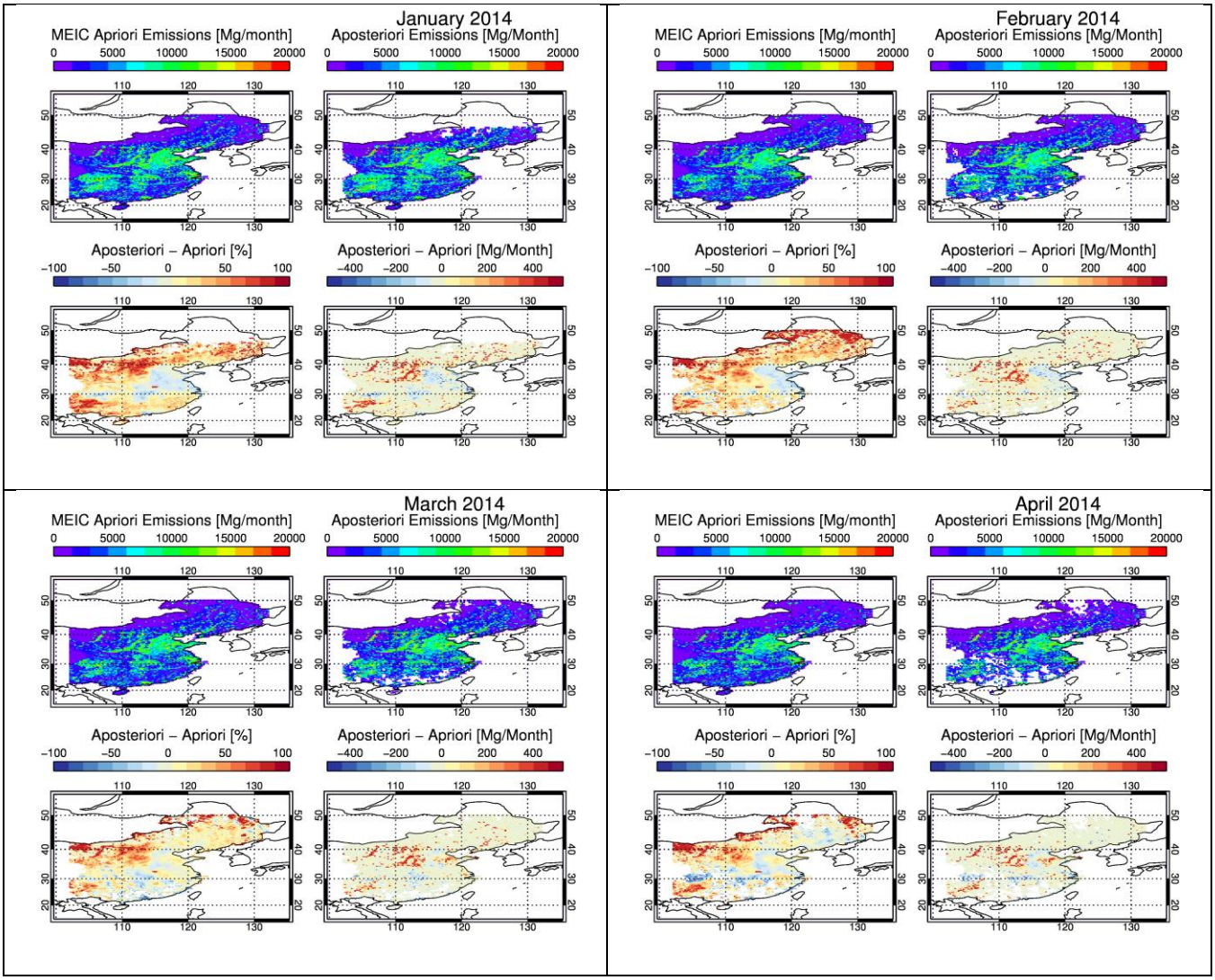

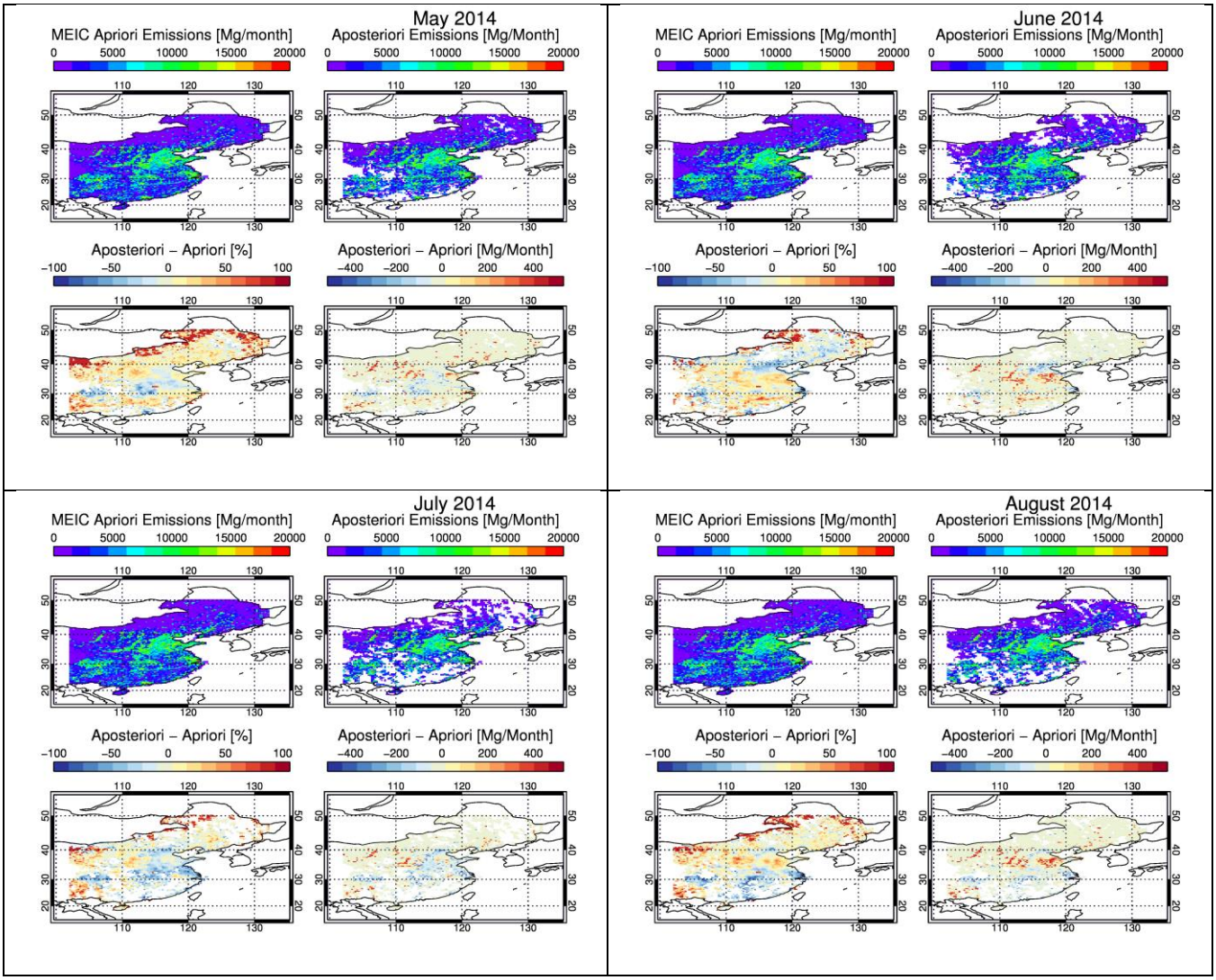
May 2014
MEIC Apriori Emissions [Mg/month]
Aposteriori Emissions [Mg/Month]
Aposteriori – Apriori [%]
Aposteriori – Apriori [Mg/Month]
June 2014
MEIC Apriori Emissions [Mg/month]
Aposteriori Emissions [Mg/Month]
Aposteriori – Apriori [%]
Aposteriori – Apriori [Mg/Month]
July 2014
MEIC Apriori Emissions [Mg/month]
Aposteriori Emissions [Mg/Month]
Aposteriori – Apriori [%]
Aposteriori – Apriori [Mg/Month]
August 2014
MEIC Apriori Emissions [Mg/month]
Aposteriori Emissions [Mg/Month]
Aposteriori – Apriori [%]
Aposteriori – Apriori [Mg/Month]

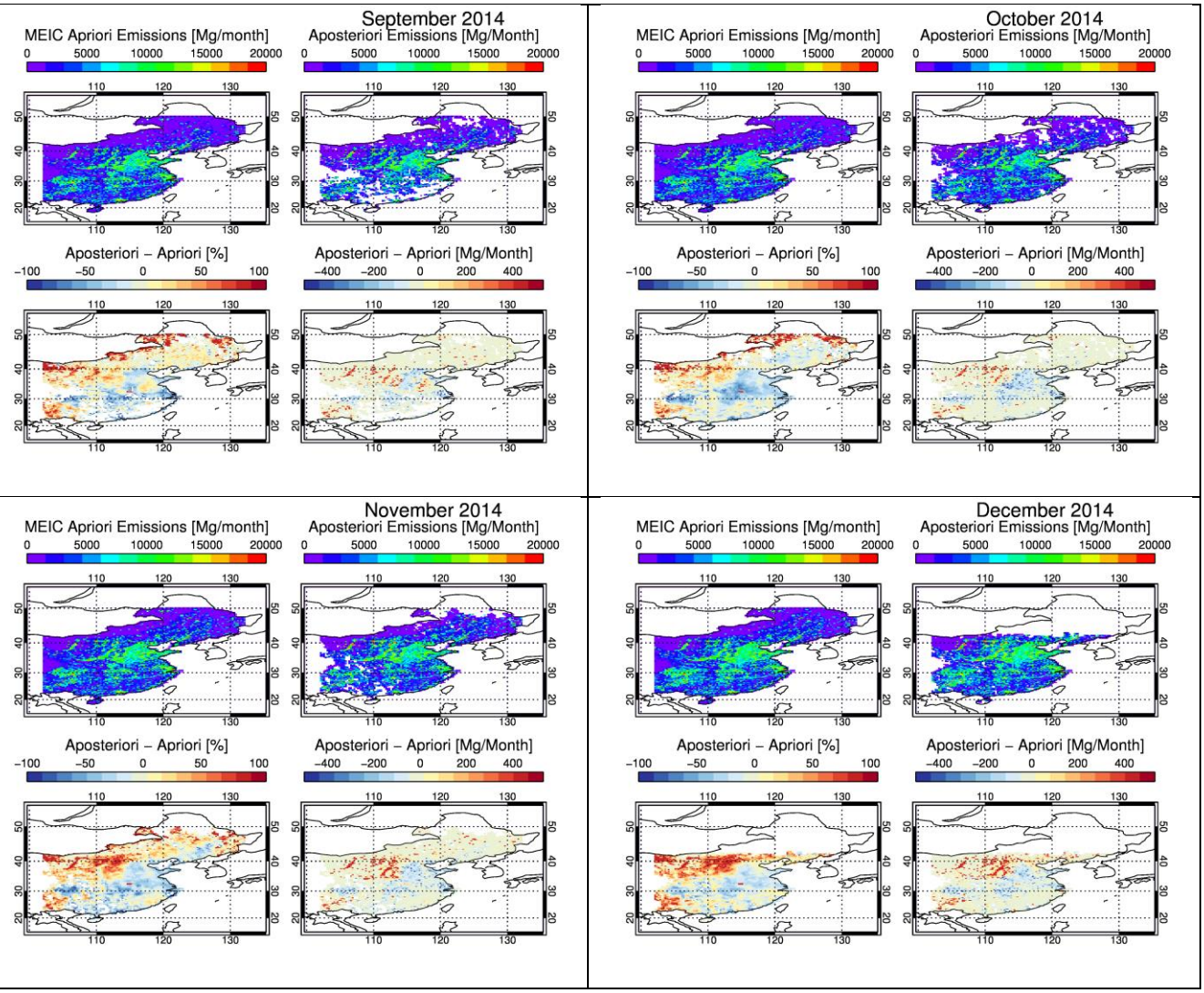
September 2014
MEIC Apriori Emissions [Mg/month]
Aposteriori Emissions [Mg/Month]
Aposteriori – Apriori [%]
Aposteriori – Apriori [Mg/Month]
October 2014
November 2014
December 2014

References

Fioletov, V. E., et al. (2011), Estimation of SO_2 emissions using OMI retrievals, Geophys. Res. Lett., doi:10.1029/2011GL049402.

Gu, D., Y. Wang, C. Smeltzer, and K. F. Boersma, Anthropogenic emissions of NOx over China: Reconciling the difference of inverse modeling results using GOME-2 and OMI measurements, J. Geophys. Res. Atmos., 119, 7732–7740, doi:10.1002/2014JD021644, 2014.

Guenther, A. B., Jiang, X., Heald, C. L., et al., The Model of Emissions of Gases and Aerosols from Nature version 2.1 (MEGAN2.1): an extended and updated framework for modeling biogenic emissions, Geosci. Model Dev., 5, 1471–1492, doi:10.5194/gmd-5-1471-2012, 2012.

Krotkov, N. A., et al. (2008), Validation of SO_2 retrievals from the Ozone Monitoring Instrument over NE China, J. Geophys. Res., 113, D16S40, doi:10.1029/2007JD008818.

Leue, C., Wenig, M., Wagner, T., et al., Quantitative analysis of NOx emissions from GOME satellite image sequences. J. Geophys. Res. 106, 5493–5505, 2001.

Levelt, P. F., G. H. J. van den Oord, M. R. Dobber, et al., The ozone monitoring instrument, IEEE Trans. Geo. Rem. Sens., 44(5), 1093–1101, doi:10.1109/TGRS.2006.872333, 2006.

Lu, Z., Streets, D. G., Zhang, Q., et al., Sulfur dioxide emissions in China and sulfur trends in East Asia since 2000, Atmos. Chem. Phys., 10, 6311-6331, doi:10.5194/acp-10-6311-2010, 2010.

Martin, R.V. et al., Global inventory of nitrogen oxide emissions constrained by space-based observations of NO2 columns. Journal of Geophysical Research 108(D17), 4537. doi:10.1029/2003JD003453, 2003.

Martin, R.V., Sioris, C.E., Chance, K., et al., Evaluation of space-based constraints on global nitrogen oxide emissions with regional aircraft measurements over and downwind of eastern North America. J. Geophys. Res. 111, D15308, doi:10.1029/2005JD006680, 2006.

Menut, L., Bessagnet, B., Khvorostyanov, D., et al., CHIMERE 2013: a model for regional atmospheric composition modelling, Geosci. Model Dev., 6, 981-1028, doi:10.5194/gmd-6-981-2013, 2013.

Theys, N., De Smedt, I., van Gent, J., et al., Sulfur dioxide vertical column DOAS retrievals from the Ozone Monitoring Instrument: Global observations and comparison to ground-based and satellite data, J. Geophys. Res. Atmos., 120(6), 2470–2491, doi:10.1002/2014JD022657, 2015.

Zhang, Q., Streets, D. G., He, K., et al., NOx emission trends for China, 1995–2004: The view from the ground and the view from space, J. Geophys. Res., 112, D22306, doi:10.1029/2007JD008684, 2007.

Zhang, Q., Streets, D. G., Carmichael, G. R., et al., Asian emissions in 2006 for the NASA INTEX-B mission, Atmos. Chem. Phys., 9, 5131–5153, doi:10.5194/acp-9-5131-2009, 2009.

Acknowledgments

Results presented in this work have been produced using the European Grid Infrastructure (EGI) through the National Grid Infrastructures NGI_GRNET (HellasGrid) as part of the SEE Virtual Organization. The authors would like to acknowledge the support provided by the Scientific Computing Office, IT A.U.Th. throughout the progress of this research work.